

Impact of the location of magnesium in zeolite-based shaped catalyst bodies on the methanol-to-hydrocarbons process

Nikolaos Nikolopoulos¹, Luke A. Parker^{2,1}, Maurits W. Vuijk, Bert M. Weckhuysen^{*}

Inorganic Chemistry and Catalysis, Debye Institute for Nanomaterials Science, Utrecht University, Universiteitsweg 99, 3584 CG, Utrecht, the Netherlands

ARTICLE INFO

Keywords:

Shaped catalyst bodies
Mg location
Methanol-to-hydrocarbons
Catalyst deactivation
Coke formation
Molecular transport
Acidity

ABSTRACT

One of the main challenges for the chemical industries is finding new ways to produce lower olefins, such as propylene and ethylene, to satisfy the increase in demand for e.g., polymers, namely polypropylene and polyethylene. The Methanol-to-Hydrocarbons (MTH) process is an alternative manufacturing process that can help to address this increasing demand for these important chemical building blocks. It has been proposed that the addition of magnesium to zeolites, in the form of powdered catalyst materials, enhances the selectivity towards light olefins. In this work, the impact of the location of magnesium (present as Mg^{2+} and MgO) in zeolite-based shaped catalyst bodies on their physicochemical properties and catalytic performance in the MTH reaction has been studied. By adjusting one of the preparation steps of the overall extrusion process in which magnesium is added tuning the location of magnesium, higher interaction between magnesium and the zeolite material could be achieved. Pre-extrusion modification showed the most favorable results in terms of physicochemical properties and catalytic activity. We found that the magnesium location could be crucial for altering molecular transport, coke formation, and catalyst deactivation during the MTH reaction due to its pronounced effects on the acidity as well as porosity of the shaped catalyst bodies. These new insights can be applied to other zeolite-based extrudate materials and other acid-catalyzed reactions as it can be crucial for the design of better and more efficient catalyst materials in their industrially shaped form.

1. Introduction

Lower olefins ($\text{C}_2\text{--C}_4$) are crucial chemical building blocks in the chemical industry as they are used to produce the necessary basic chemicals, such as propylene oxide, as well as a wide variety of polymers [1,2]. Considering the increasing demand for polyethylene and polypropylene and the transition towards fossil-free chemical building blocks, new ways to produce light olefins are needed [1]. The Methanol-to-Hydrocarbons (MTH) process offers an alternative route to produce lower olefins, such as ethylene and propylene, in which methanol and/or dimethyl ether is converted to olefins and gasoline-range products [3–6].

The MTH reaction is an acid-catalyzed reaction in which various zeolites and zeotypes have been studied as catalyst materials during the past decades [3]. ZSM-5 and SAPO-34 zeolites have proven to be the most promising solid catalysts. Even though both of these catalysts are great for the MTH process, they have striking differences in their

catalytic performance [3,5,7–9]. Zeolite framework structures with small-sized pores, e.g., SAPO-34 (with CHA framework structure), exhibit high selectivity towards light olefins, while they deactivate relatively fast. In contrast, zeolite framework structures with medium-sized pores, such as ZSM-5 (with MFI framework structure), are more stable and less prone to deactivation, while also having a much larger product distribution (i.e., the formation of light olefins and aromatics) [3,10,11].

There are many strategies to enhance the selectivity towards ethylene and propylene and both acidity and porosity play a crucial role. Firstly, a facile way to increase olefin yields is to regulate the reaction conditions, such as low pressures and high reaction temperatures. Altering the strength and the density of acid sites by modifying the Si/Al ratio has been another approach to increase the production of lower olefins [12,13]. Post-synthetic modifications, such as dealumination and/or desilication, can influence selectivity and the lifetime of the catalyst [7,9,14–23]. Metal doping is proven to help enhance the

^{*} Corresponding author.

E-mail address: b.m.weckhuysen@uu.nl (B.M. Weckhuysen).

¹ Authors contributed equally in this work.

² Current affiliation: TNO Environmental Modelling, Sensing and Analysis, Princetonlaan 6, 3584 CB Utrecht, The Netherlands.

efficiency of the MTH process. Alkaline earth metal (e.g., Mg, Ca, Sr, and Ba), rare earth metals (e.g., La), transition metals (e.g., Co, Ni, Fe, and Zr), and other chemical elements, such as B and P, are, among others, used to achieve higher selectivity to light olefins [20,24–37].

Chen et al. studied the effect of Mg modification on ZSM-5 zeolites for the methanol conversion. Mg addition reduced the number of strong acid sites, while new medium strength acid sites were created. Regarding the catalytic performance, Mg-modified ZSM-5 zeolites exhibited enhanced propylene selectivity and possessed increased lifetime [38]. Similar results were found in a study of Bakare et al., in which the effect of alkaline earth metals, such as Ca, Mg, and Ba, was investigated. Their research also revealed the formation of extra Lewis Acid Sites (LAS) [25]. Goetze et al. have investigated and compared the coke formation of H-ZSM-5 and Mg-ZSM-5 zeolites using *operando* UV–Vis spectroscopy. It was found that Mg-ZSM-5 showed a prolonged lifetime due to the slower progression of the coke front along the catalyst bed. The latter can be attributed to decreased Brønsted acidity, which hinders the formation of secondary coke [24]. Yarulina et al. confirmed these findings as it was revealed that propylene selectivity is firmly related to the isolation of Brønsted Acid Sites (BAS), while the formation of LAS upon addition of Mg or Ca inhibits reactions, involving aromatic moieties and, thus, prevents coke formation [30].

It is important to mention here that the majority of the studies in the literature are based on zeolite powder samples, and only a few studies shed light on shaped multi-component catalyst bodies, which are often the real catalyst material used in an industrial reactor. Pérez-Ramírez et al. investigated the impact of various binders on the performance of zeolite ZSM-5-based technical catalyst materials in the MTH reaction. Attapulgite (which is a magnesium aluminum phyllosilicate clay) has been shown to prolong the lifetime of the catalyst material and increased the selectivity towards light olefins. The authors attributed these observations to mobile Mg species migrating from the attapulgite binder to the zeolite [39]. De Jong's group has underlined the importance of nanoscale intimacy in a bifunctional zeolite-binder catalyst for the conversion of hydrocarbons. They showed that the control over Pt location on the zeolite or binder significantly influenced the catalytic performance [40–43].

Nonetheless, the influence of Mg in zeolite-based catalyst materials on the MTH reaction has not been investigated thoroughly. To the best of our knowledge, the effect of Mg location in zeolite-based extrudates on the methanol conversion has not yet been studied. Here, by tuning the Mg location in zeolite alumina-bound shaped catalyst bodies, and, thus, the interaction between Mg and zeolite and/or binder has been investigated. To accomplish this goal, three different approaches for Mg addition have been followed; namely before, during, and after the extrusion process. Altering the step in which Mg was added (i.e., pre-, during, and post-extrusion) was crucial for the physicochemical properties of the technical catalyst bodies and their performance in the MTH reaction. The pre-extrusion modification resulted in a prolonged lifetime and large increase in the yield of light olefins due to a better Mg-zeolite interaction. A clear and distinct link was established between acidity, molecular transport, and deactivation during the MTH process.

2. Experimental section

2.1. Chemicals and materials

The following chemicals, gases, and materials were used: methanol (Acros, HPLC grade, 99.99% pure), N₂ (Linde, 99.998%), He (Linde, >99%), Ar (Linde, 99.998%), methylcellulose (Sigma Aldrich, 4000 CP), acetic acid (Sigma Aldrich, 99.5%), boehmite (CATAPAL D, SASOL), Zeolite HZSM-5 (Zeolyst, 3024E), magnesium nitrate (Mg(NO₃)₂ 6H₂O, Sigma Aldrich, 99%), and magnesium oxide (MgO, Sigma Aldrich, 99%).

2.2. Materials preparation

2.2.1. Preparation of shaped catalyst bodies

Unmodified or modified powder H-ZSM-5 and boehmite were mixed in a 50-50 wt% zeolite-to-binder ratio. Methylcellulose was added and further mixed to acquire a homogeneous solid mixture. Acetic acid diluted in ultra-pure water was then added to form a paste. A Mini-Screw Extruder (Caleva) equipped with a 2-mm-diameter die plate with a cylindrical shape was used to extrude the paste. The formed catalyst extrudates were dried in air overnight, followed by a calcination step in a tubular oven at 600 °C for 6 h (with a ramp of 1 °C/min) in a flow of air. In the case of Mg addition during the extrusion process, the proper amount of MgO powder, to achieve a loading of 0.5 and 1 wt%, was added at the same moment together with the unmodified powder H-ZSM-5 and boehmite.

2.2.2. Mg impregnation method

Mg modification of ZSM-5 and boehmite powder, as well as zeolite-alumina catalyst extrudates, was done by wet impregnation. In brief, the proper amount of magnesium nitrate hexahydrate (aiming for 0.5 and 1 wt% of Mg in the final samples) was dissolved in 15 ml of ultra-pure water and added with the support in a round-bottom flask. The mixture was left to mix for 10 min to ensure homogeneity. The round-bottom flask was attached to a rotary evaporator, and vacuum was applied until the water was evaporated and the support was dry. The samples were calcined at 550 °C for 4 h (with a ramp of 1 °C/min). This synthesis method was used to prepare the individual Mg-modified components, such as ZSM-5 and boehmite (further denoted as the pre-extrusion modification). Furthermore, zeolite-alumina catalyst extrudates were impregnated in the same way (further termed as the post-extrusion modification).

2.3. Materials characterization

N₂ physisorption was performed using a Micromeritics TriStar 3000 instrument operating at liquid N₂ temperature. Before the measurements, a drying step was applied at 300 °C under an N₂ flow for 15 h. Ammonia Temperature-Programmed Desorption (NH₃-TPD) was measured on a Micromeritics AutoChemII 2920 instrument. X-ray diffraction (XRD) was measured on a Bruker D2 X-ray powder diffractometer with a Co K α X-ray tube ($\lambda = 1.7902$ Å) as the source. The imaging of the spent catalyst samples after the MTH reaction was done using Confocal Fluorescence Microscopy (CFM), and the procedure followed is described in detail elsewhere [44].

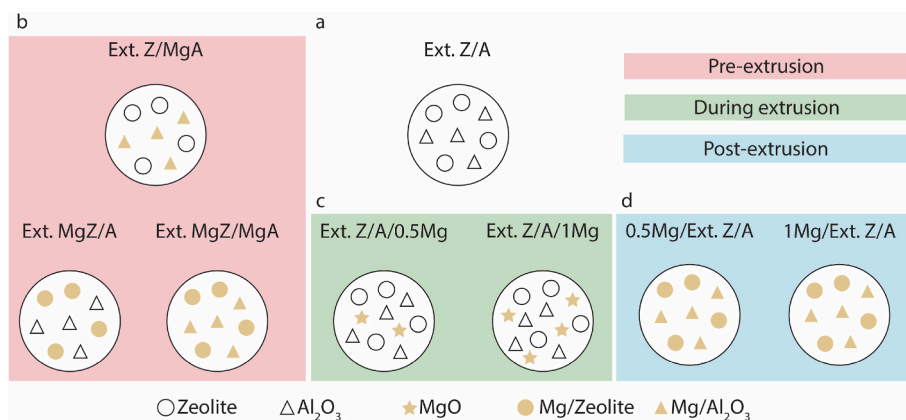
2.4. Catalytic testing

The performance of the various catalyst samples under study for the MTH reaction was tested in an *operando* UV–Vis Diffuse Reflectance Spectroscopy (DRS) set-up. ~69 mg of catalyst was placed in a fixed-bed reactor operating at a Weight Hourly Space Velocity (WHSV) of 6 h⁻¹ at 400 °C. Methanol and the products formed during the reaction were detected using an Interscience Compact Gas Chromatograph (GC). More details of the set-up can be found elsewhere [11,24].

3. Results and discussion

In this study, we investigated the effect of the location of Mg in zeolite-based catalyst extrudates. Three different synthesis approaches were chosen to modify the zeolite-alumina shaped catalyst bodies with Mg. These methods are summarized in Scheme 1 and Table S1. In these methods, Mg was introduced as both Mg²⁺ and MgO and is likely present as a mix of both Mg²⁺ ions and MgO in the final catalysts. When we refer to Mg we are referring to all potential Mg species present and not suggesting that Mg is present in the metallic form.

Firstly, Mg was added to the individual components, such as zeolite



Scheme 1. Sample overview of the different catalysts synthesized, characterized, and tested. Schematic representation of the samples and the three different synthesis approaches followed.

and/or binder, before extrusion, in the so-called pre-extrusion-addition. In this case, Mg was impregnated in the ZSM-5 zeolite (further denoted as MgZ) and/or the alumina precursor binder (further denoted as MgA). Then, the modified samples were used to make the shaped catalyst bodies. The samples that belong in this category are: a sample which consists of Mg impregnated zeolite (MgZ) and unmodified alumina binder (A) (further denoted as Ext. MgZ/A), a sample with unmodified zeolite (Z), and Mg impregnated alumina (MgA) (further denoted as Ext. Z/MgA), and, finally, a sample with Mg impregnated zeolite (MgZ) and Mg impregnated alumina (MgA) (further denoted as Ext. MgZ/MgA). Secondly, the addition of Mg was done during the extrusion process, in the so-called during-extrusion-addition. Mg was added in the form of MgO, and it was mixed with the unmodified zeolite material and binder

powders during the extrusion process. The samples are denoted as Ext. Z/A/0.5 Mg and Ext. Z/A/1 Mg where 0.5 and 1 represent the wt% of Mg in the sample. Thirdly, Mg modification was performed after the extrusion process, in the so-called post-extrusion-addition. In this case, unmodified zeolite and binder powder samples were used to make technical catalyst bodies, and then Mg was impregnated in the extrudates. The samples are further denoted as x/yMg/Ext. Z/A, where x and y represent the amount of Mg in the final sample.

We used Scanning Electron Microscopy with Energy-dispersive X-ray spectroscopy (SEM-EDX) to validate the synthesis method and the location of Mg on selected samples. The results are shown in Figs. S1–3. Regarding the pre-extrusion modification, point spectra in zeolite and/or alumina binder-rich areas proved the presence of Mg only in the

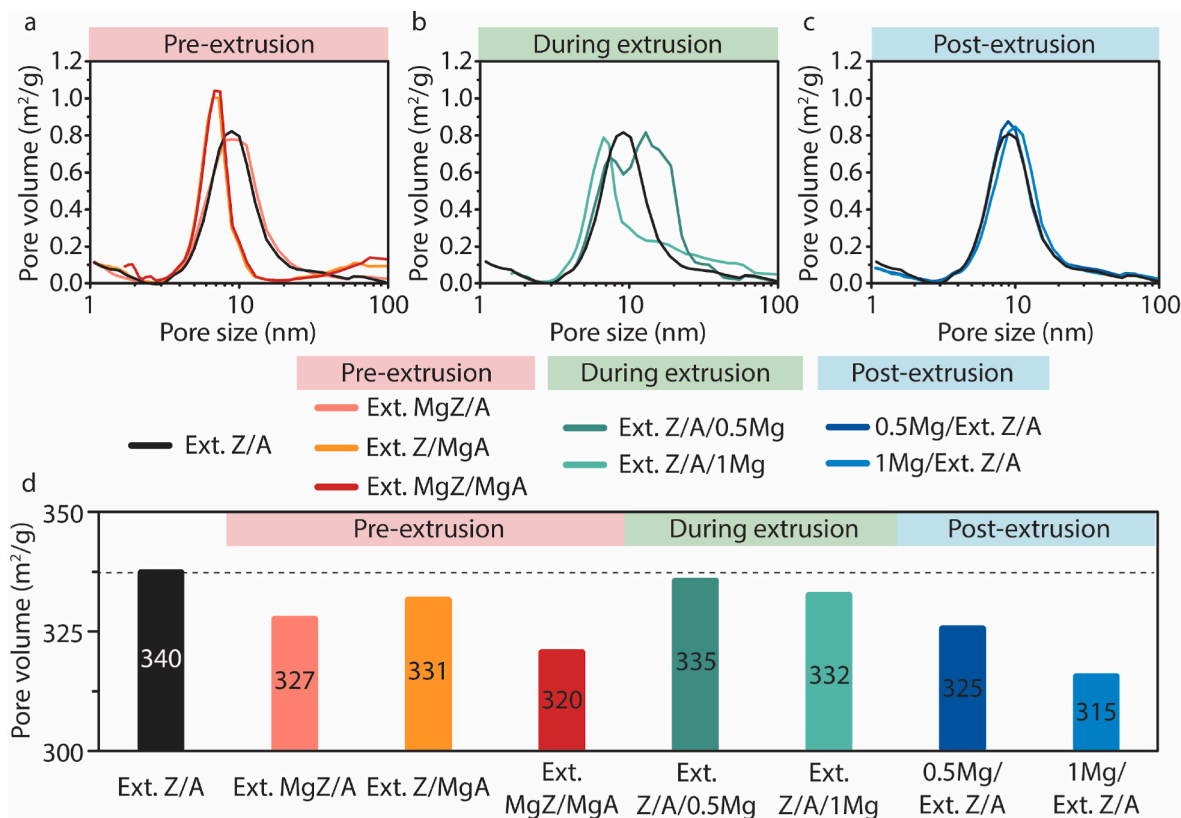


Fig. 1. Overview of the textural properties of the zeolite-based materials upon Mg modification. a), b), and c) pore volume distribution (logarithmic x-axis) of the samples modified with Mg prior, during, and after the extrusion process, d) BET surface area of all samples, separated in the three categories, namely the pre-extrusion-addition, the during-extrusion-addition and the post-extrusion-addition.

zeolite for the Ext. MgZ/A sample and only in the binder for the Ext. Z/MgA. SEM-EDX for the Ext. Z/A/1 Mg sample shows larger agglomerates of Mg and no presence of Mg in zeolite and/or the alumina binder. Lastly, Mg appears in the zeolite and/or the alumina binder for the 1Mg/Ext. Z/A sample.

Fig. 1 provides an overview of the textural properties of the shaped catalyst bodies before and after the addition of Mg as a function of the three ways of preparation. The reference catalyst extrudate sample has a bimodal pore size distribution. A first small peak is observed at 1 nm which appears to be the tail of a peak, suggesting the presence of pores <1 nm. This is attributed to the presence of micropores, associated with the zeolite material. The second peak centered at ~8 nm is attributed to the presence of mesopores, most probably from the alumina binder and interparticle domains formed upon extrusion, such as zeolite-binder and/or binder-binder interactions. Regarding the pre-extrusion-addition, Fig. 1a and Fig. S4 indicate that when only the zeolite was impregnated prior to extrusion (Ext. MgZ/A, pink color), a lower amount of micropores of ~1–2 nm is observed, resulting in a subsequent slight decrease in surface area (Fig. 1d). When Mg is added before extrusion with the alumina binder, the second peak is shifted to pores of smaller sizes. Regarding the Ext. Z/MgA and the Ext. MgZ/MgA materials, the boehmite, used as alumina precursor, was impregnated with Mg and then calcined before using it for extrusion. Thus, it can be expected that strong interaction between Mg-boehmite can be achieved and Mg will fill the porous structure of Al_2O_3 and decrease its porosity. Similar results have been found in literature when Mg- Al_2O_3 has been evaluated as catalytic support in a hydrodesulphurization reaction [45]. The authors claim that when Mg is introduced, a mixed Mg-Al oxide is formed which fills the surface of the alumina support material. An alternative explanation could be that Mg addition before extrusion prevented the formation of interparticle pore space between zeolite-binder or binder-binder materials. Moving to the addition of Mg during the extrusion process, the Ext. Z/A/0.5 Mg sample shows an extra third peak centered at ~10.5 nm. An increase of the Mg amount to 1 wt % shows a decrease of the extra third peak and further decrease in the

pore size as the peak at ~8 nm shifts to smaller pore size (~6 nm).

However, as shown in Fig. 1d, the addition of Mg during the extrusion process showed no significant effect on the surface area. All the findings mentioned above imply that Mg mainly interacts with the alumina binder in this approach. Lastly, Mg impregnated in the extrudate samples (i.e., the post-extrusion-addition samples) shows a minor decrease in the amount of micropores (Fig. 1c) as well as in the total surface area (Fig. 1d), suggesting blockage of the zeolite pores during the impregnation process.

All the extrudate samples, i.e., both the unmodified and Mg-modified ones, show a crystal phase characteristic of an MFI topology, as shown in Fig. 2, as assessed by X-ray Diffraction (XRD) [38]. No significant framework change on the samples can be noticed upon adding Mg. Further inspection of the XRD patterns shows a lack of additional peaks related to the presence of Mg species, which can be justified by the low content of Mg (0.5–1 wt%) and/or the high level of Mg dispersion. Regarding the samples in which Mg was added before extrusion (Fig. 2a and Fig. S5), the Ext. MgZ/A and Ext. MgZ/MgA samples showed a decrease in the overall XRD intensity. The impregnation of metals in zeolites ZSM-5 is known to decrease the overall crystallinity due to the formation of defects and dealumination [46].

However, when only the binder is impregnated with Mg (Ext. Z/MgA, orange color), no decrease in XRD intensity is observed compared to the reference sample. The observations mentioned above are implicit of the interaction between Mg and zeolite materials. On the other hand, when Mg is added during the extrusion process (Fig. 2b and Fig. S5), no major differences can be found compared to the reference sample, which implies no or poor interaction between Mg and the zeolite. Furthermore, as illustrated in Fig. 2c and Fig. S5, post-extrusion modification of extrudates with Mg also shows a decrease in the XRD peak intensities correlated to an increasing amount of the Mg loading.

The Ammonia Temperature-Programmed Desorption (NH_3 -TPD) experiments, of which the results are summarized in Fig. 3, were used to measure the total amount of acid sites as well as their strength. Furthermore, the NH_3 -TPD curves were deconvoluted and used to

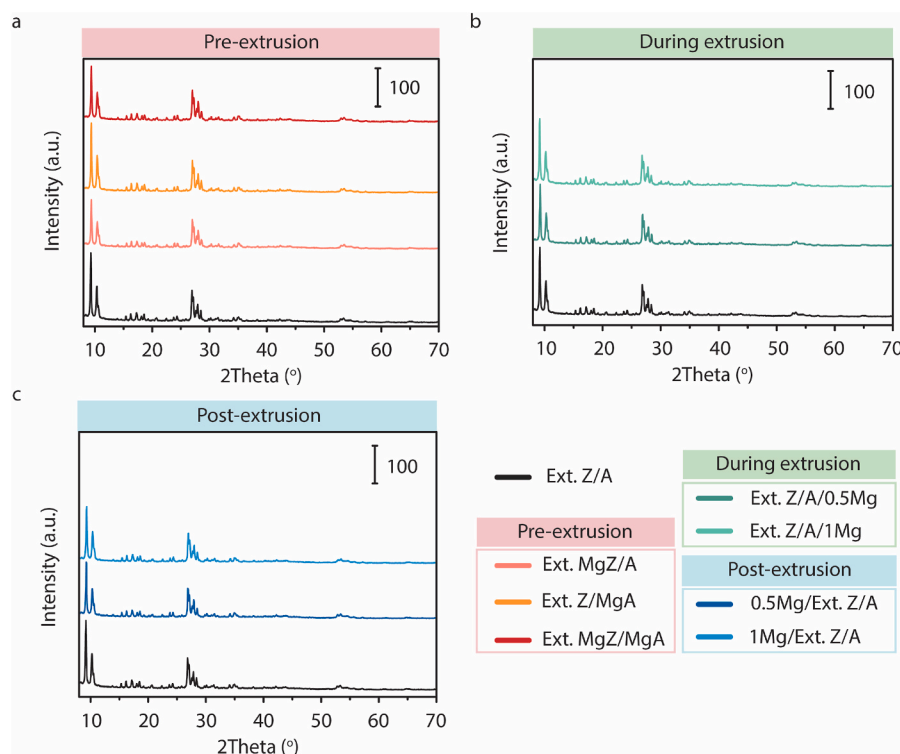


Fig. 2. Overview of the structural changes of the zeolite-based materials upon addition of Mg. X-ray Diffraction (XRD) patterns of the samples modified with Mg a) pre-extrusion, b) during the extrusion, and d) post-extrusion.

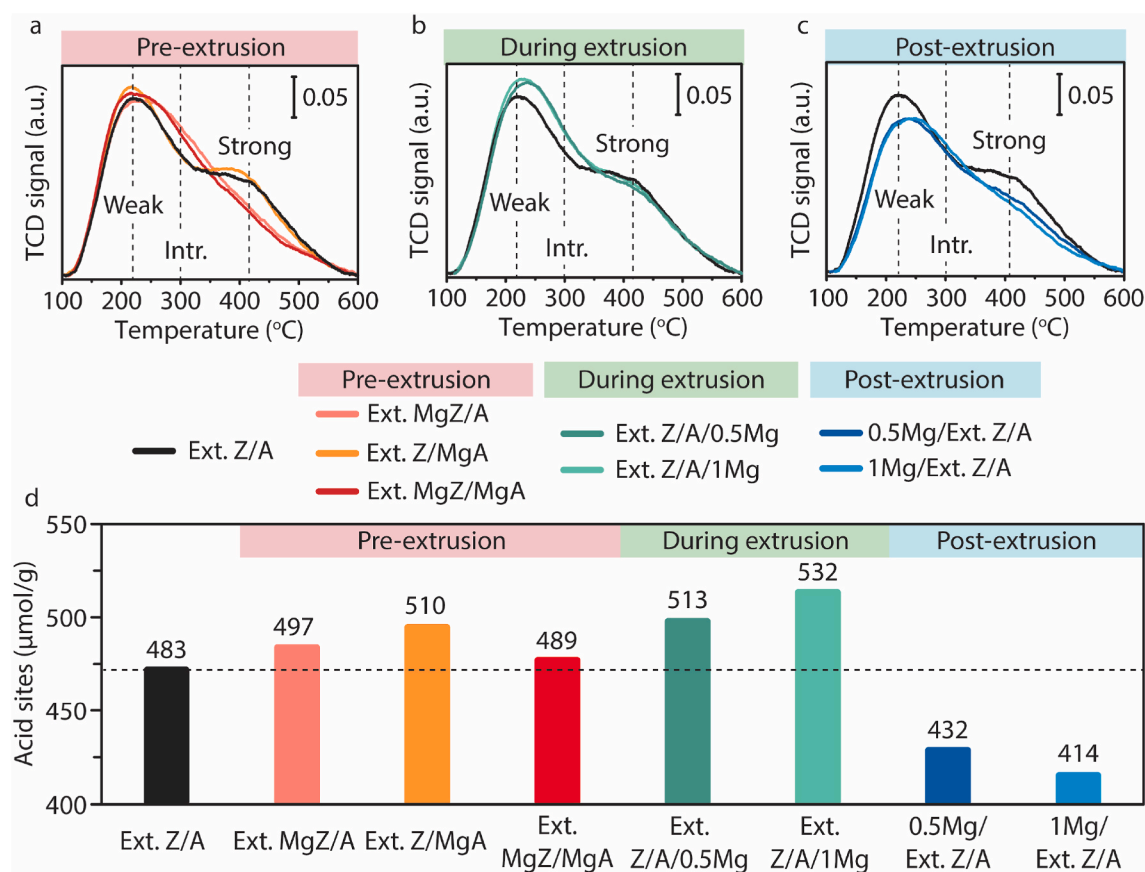


Fig. 3. Overview of the acidic properties of the zeolite-based materials upon Mg addition. Ammonia Temperature-Programmed Desorption (NH_3 -TPD) analysis of the samples modified with Mg a) prior, b) during, and c) after the extrusion process. d) Number of acid sites ($\mu\text{mol/g}$) of all samples.

quantify the amount of weak, intermediate and strong acid sites, which is illustrated in Fig. S6. The reference sample shows two major TPD peaks, centered at $\sim 220^\circ\text{C}$ and $\sim 410^\circ\text{C}$. According to literature, the first peak is attributed to the presence of weak acid sites, while the second is due to the presence of strong acid sites [47–50]. In previous reports, zeolite modification using Mg affected the overall acidity of the samples [24,30,38]. Firstly, regarding the pre-extrusion modification (Fig. 3a), the sample when only the zeolite is impregnated with Mg (Ext. MgZ/A, pink color) shows a significant decrease in the number of strong acid sites. This is likely due to Brønsted acid sites being exchanged for Mg^{2+} cations. The addition of Mg resulted in an increase in the number of weak acid sites as well as in the formation of extra intermediate strong acid sites. Similar results were noticed for the sample where both components were impregnated with Mg before extrusion (Ext. MgZ/MgA, red color). Unexpectedly, impregnating only the binder material resulted in an increased strong acidity, but also in the formation of weak acid sites. Even though the increase of the number of weak acid sites could be expected, as Mg species acts as LAS [24,30,38], the formation of strong acid sites are clearly not. However, the latter observation could be explained by the migration of Al species from the binder material to the zeolite framework, which is also reported in the literature [51,52]. Mg modification of the samples prior to the extrusion process causes an increase in the total amount of acid sites, as shown in Fig. 3d. At the same time, the relative ratio between weak, medium, and strong acid sites vastly differs among the samples under study. To further assess the changes in acidity resulting from the addition of Mg during the extrusion process (Fig. 3b), our NH_3 -TPD measurements show that there is an increase in weak and medium acidity, while there is a minor decrease in the number of strong acid sites. The latter implies no significant Mg-zeolite interaction. It can only be assumed that the increase of weak and medium acidity is due to the presence of Mg

species.

On the other hand, the decrease in the number of strong acid sites is due to the interaction of Mg species with the acid site of the external zeolite surface or the migration of Mg species in the zeolite pores. The post-extrusion modification showed a decrease in the overall acidity (Fig. 3d), especially of the weak and the strong acid sites, and the formation of intermediate acid sites (Fig. 3c). This could arise from a combination of Mg exchanging with BAS in the zeolite, as well as blocking pores and lowering the overall accessibility to acid sites. Based on the results as mentioned earlier, the pre-extrusion modification with Mg shows the highest level of interaction, as shown from the XRD and NH_3 -TPD measurements performed. This can be concluded from the decreased overall relative intensity in the XRD pattern when Mg is impregnated in the zeolite. At the same time, NH_3 -TPD experiments showed a significant loss of the number of strong acid sites and the formation of new medium-strong acid sites. Weak interaction between Mg and the zeolite material was achieved in the post-extrusion impregnation. Zeolite-based extrudate catalyst materials are known to suffer from pore blockage phenomena, which makes diffusion of Mg precursor more difficult and causes further pore narrowing [51,53]. On the other hand, Mg-ions added to the technical catalyst bodies during the extrusion lead to a minimum interaction between Mg and the zeolite.

The samples were tested on the activity and selectivity in the MTH reaction in order to investigate the effect of Mg modification in the zeolite-based alumina-bound shaped catalyst bodies on their catalytic performance. Fig. 4 illustrates the methanol conversion and the yield of the ethylene and propylene formed during the MTH reaction operating at a Weight Hourly Space Velocity (WHSV) of 6 h^{-1} and 400°C for 35 h Time-on-Stream (TOS). The reference sample (Ext. Z/A, black color), as Fig. 4a illustrates, exhibits a high level of conversion at $\sim 94\%$. However, the methanol conversion decreased fast and reached a value of $\sim 84\%$

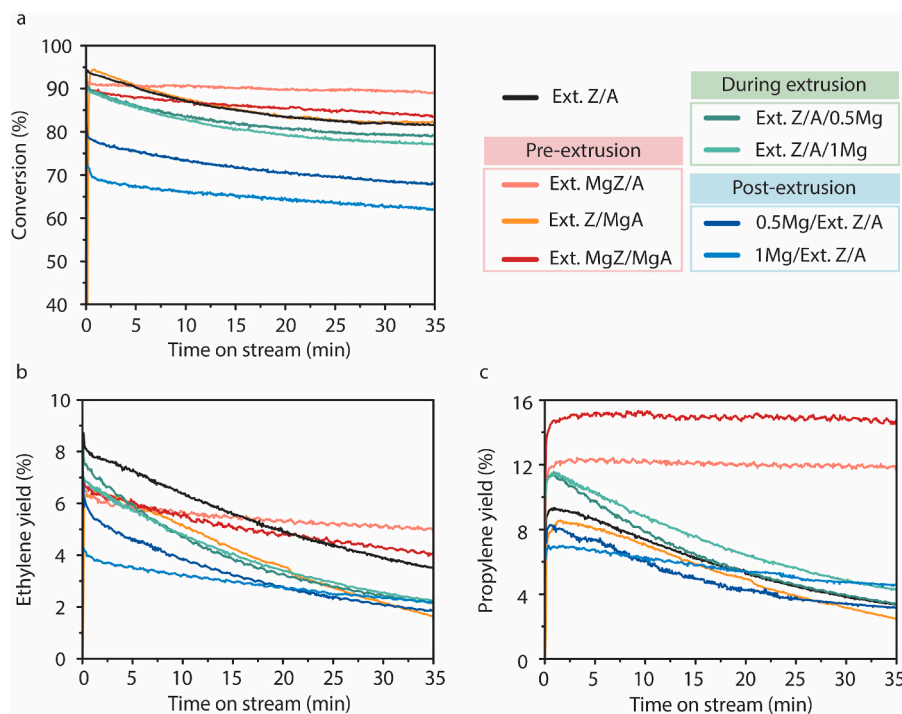


Fig. 4. Overview of the catalytic performance of the zeolite-based materials in the absence and presence of Mg for the Methanol-to-Hydrocarbons (MTH) reaction. Activity and yields of all extrudate samples versus time on stream for the MTH reaction conducted at 400 °C with a Weight Hourly Space Velocity (WHSV) of 6 h⁻¹. a) Methanol conversion, b) yield of ethylene, and c) yield of propylene.

within the first 20 h TOS. The same trend is observed for the sample in which Mg is impregnated only in the alumina binder, which implies that Mg species present in the binder and the slight increase in acidity have no effect on the methanol conversion. Ext. MgZ/A (pink color) and Ext. MgZ/MgA (red color) samples can achieve a high level of conversion ~92 and ~89%, respectively. Although this is slightly lower than the reference sample and Ext. Z/MgA sample, the decrease of strong acid sites can explain this due to Mg addition. Impregnating the zeolite with Mg before extrusion shows a prolonged lifetime as both samples are less prone to deactivation as they preserve a higher level of conversion than the reference sample. This is in line with findings in literature that show Mg addition reduces strong acidity, increasing the catalyst's stability [24,30,38].

Regarding the samples in which Mg is added during extrusion (Ext. Z/A/0.5 Mg, dark green color, and Ext. Z/A/1 Mg, light green color), it can be seen that they achieve a lower level of conversion compared to the reference material. This can be explained by the decrease in surface area, as well as the minor decrease in the strong acidity, as shown in Figs. 1b and 3b, respectively. Further decrease in the conversion was observed for the samples in which Mg was impregnated after the extrusion process, with the sample containing 1 wt% exhibiting ~70% of methanol conversion.

Nonetheless, the reference sample showed similar trends in ethylene and propylene yield. On the contrary, the Ext. Z/MgA (Mg impregnated only in the binder) sample exhibited the same yield of propylene at the same time as decreased ethylene yield underlying the major effect of the properties of the binder. As in this case, Ext. Z/MgA (orange color) sample showed pores of smaller size, while the Mg addition foresees the basicity of the binder. These changes promote the olefin cycle over the aromatic cycle. Mg modification of only the zeolite before extrusion (Ext. MgZ/A, pink color) resulted in a ~133% increase in propylene yield and a simultaneous decrease in ethylene yield. Impregnating both components prior to extrusion (Ext. MgZ/MgA, red color) caused an increase in propylene yield (~166%). These findings also point out that Mg present in the binder holds a crucial role in the selectivity towards

light olefins. Even though Mg and zeolite have little interaction when Mg is added during the extrusion process, based on the physicochemical characterization and the results mentioned above, it can be seen that Ext. Z/A/0.5 Mg and Ext. Z/A/1 Mg samples favored the propylene formation. Post-extrusion modification produced lower yields of ethylene and propylene in total due to the lower conversion levels recorded in these sets of samples. However, it can be seen that propylene formation is favored over ethylene due to the presence of intermediate strong acid sites. Last but not least, Fig. S7 illustrates the selectivities towards ethylene (black), propylene (red), C₄ olefins (blue), C₅ olefins (pink), and paraffins (sum of methane, ethane, propane, C₄, and C₅) (green) of all samples under study versus TOS for the MTH reaction. The latter was done in order to rule out any possibility to mislead due to the fact that the yield could be affected by the different conversion levels. Similar trends were noted for ethylene and propylene selectivities as those described above for the yields. Moreover, the paraffins selectivity draws great interest. We note that the reference sample (Ext. Z/A) exhibits the higher selectivity towards paraffins which can be attributed to the high content of strong acid sites. Relatively high selectivity towards paraffins can also be noted for sample Ext. MgZ/A in which Mg is added only in the zeolite before extrusion. In parallel, it can be seen that in all the other samples in which Mg is added either in the binder prior to extrusion, during, and/or after extrusion, the selectivity towards paraffins is considerably lower compared to Ext. Z/A and Ext. MgZ/A samples. A representative example is Ext. Z/MgA (in which only the binder is modified with Mg) and it can be noted that it exhibits ~10% less selectivity towards paraffins compared to the reference sample (Ext. Z/A). Hydrogen transfer reactions could take place in acid sites located in the alumina binder that could lead to the formation of aromatics and alkanes. The above mentioned observation could imply that modification of the binder with Mg can inhibit these type of successive reactions leading to lower selectivity towards paraffins. This consideration underlines the importance of the presence of the binder as well as its properties in the physicochemical properties and the catalytic performance in the MTH reaction. The zeolite powder material and Mg-

modified zeolite powder was also tested and compared for the MTH reaction, as shown in Fig. S8. The latter experiments confirmed the beneficial effect of Mg in the catalytic activity and the increase towards propylene.

To further understand the effect of Mg, Thermogravimetric Analysis (TGA) measurements were performed on a sample modified by each approach (pre-extrusion, during extrusion, and post-extrusion) with 0.5 wt% of Mg and the reference sample after 35 h time on stream. As illustrated in Fig. 5a, the TGA curves for every sample showed a low-temperature weight loss at below 150 °C and a high-temperature weight loss at above 150 °C, which are attributed to removal of water and coke, respectively. The reference sample, the sample in which Mg was impregnated prior to extrusion, and the one in which Mg was added during extrusion showed a similar amount of weight loss. On the contrary, the 0.5Mg/Ext. Z/A shows lower weight loss.

To further evaluate the differences in the deactivation of these samples, the individual percentages of the two types of weight losses (low- and high-temperature) are presented in Fig. 5b. Focusing on the coke content, it is clear that the Mg addition reduces the formation of coke deposits. Post-extrusion modification showed less formation of coke, which can be ascribed to the lower methanol conversion levels. Comparing Ext. MgZ/A and Ext. Z/A/0.5 Mg samples, it is obvious that higher interaction reduces further the coke formation. The CO₂ fragment signal is plotted against the temperature and shown in Fig. 5c to gain more insights into the type of coke species formed during the reaction. The reference sample shows different coke species that can be separated into two categories, the “soft” and “hard” coke. “Soft” coke can consist of smaller aromatic compounds, such as alkylated benzenes and naphthalene, which need a lower temperature to burn off, while “hard” coke can consist of larger polyaromatic compounds and even graphite-like coke which need higher temperatures to be removed. Comparing the reference sample with the one pre-extrusion modified, it is clear that Mg-zeolite interaction strongly reduces the formation of “hard” coke. The reduction of strong acidity and the formation of moderate strong acid sites play a significant role in the coke species formed. However, the samples 0.5Mg/Ext. Z/A (dark blue) and Ext. Z/A/0.5 Mg (dark green) both show the presence of “soft” and “hard” coke with “hard” coke dominating.

Confocal Fluorescence Microscopy (CFM) was used to visualize the nature of the coke species and their spatiotemporal distribution throughout the catalyst extrudate in the spent unmodified and modified

samples after 15 and 75 min TOS in the MTH reaction. Various reaction products can be formed during the MTH process. These products can be separated into “less conjugated” species, such as alkylated benzenes and naphthalene, and “more conjugated”, such as alkylated phenanthrenes (PH), pyrenes (PY), and (LPAs). Two lasers (i.e., 488 and 642 nm) were used to detect and separate the two types of reaction products. Green fluorescence can be emitted from the “less conjugated” species, while red fluorescence originates from the “more conjugated” species.

The top-view 3D CFM images of the reference sample, as shown in Fig. 6a, show the presence of two different color areas, which translates into different types of coke deposits. After 15 min TOS, a green/yellow fluorescent near-edge region exists in the catalyst extrudates, while the core of the catalyst extrudates shows an orange fluorescence. The green/yellow color in the near-edge region indicates the presence of “less conjugated” hydrocarbon species, while the orange core region indicates the presence of “more conjugated” hydrocarbon species. According to the literature, there is a molecular transport boundary towards the core of the catalyst extrudate [44,54]. Thus, “less conjugated” species produced in the core of the catalyst extrudate in their way to diffuse out can fall into secondary oligomerization reactions to form larger and more conjugated species, which are trapped in the core of the catalyst extrudate, explaining the orange core of the extrudate. The existence of less conjugated species in the near-edge region (bearing a green/yellow fluorescent color) could be explained by the cracking reaction of larger species to form smaller aromatic species. At 75 min TOS, it is evident that the two coke regions are still present, and their colors are more red due to the larger conjugated species formed.

Upon adding Mg during the extrusion process, as illustrated in Fig. 6c, no major change in the nature and the distribution of coke species is observed in the 15 min spent samples. After 75 min TOS, the near-edge and the core regions of the catalyst extrudate show less red color, implying the formation of smaller aromatic species upon addition of Mg. Regarding the Ext. Z/A/1 Mg sample, it is clear that the near-edge region is thicker. N₂ physisorption results and pore volume distribution showed a decrease in mesoporosity, which could explain the thickening of the near-edge region. The latter is in line with the literature as Whiting et al. reported that a decrease in porosity and accessibility resulted in the trapping of larger molecules in the core of the zeolite-containing catalyst extrudates [44]. Similar results regarding the thickness of the near-edge region were observed for the post-extrusion modified samples. After 75 min TOS, both samples, 0.5Mg/Ext. Z/A

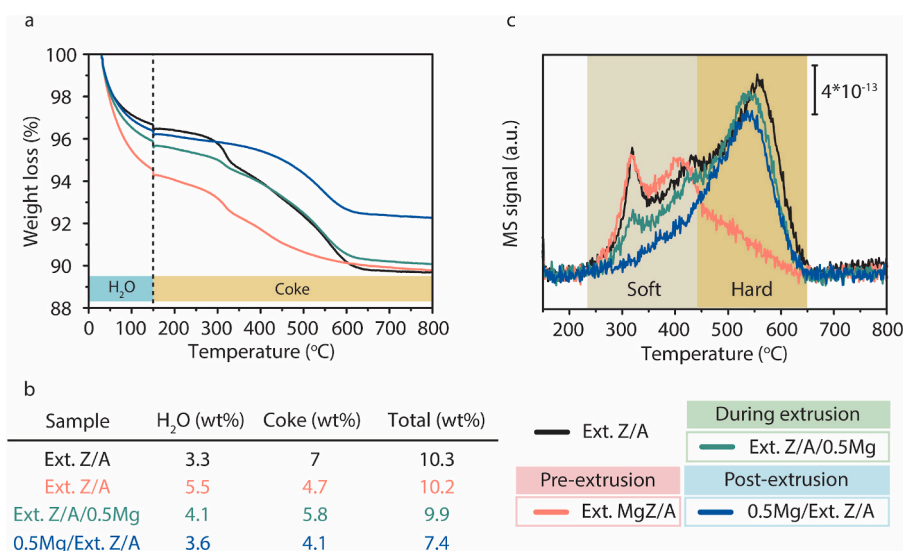


Fig. 5. Amount and nature of coke formed on the spent samples. a) Thermogravimetric Analysis (TGA), b) Table containing of H₂O, coke, and total weight loss and c) CO₂ ($m/z = 44$) fragment versus temperature for the reference sample (Ext. Z/A, black), the sample in which Mg is impregnated in the zeolite prior to extrusion (Ext. MgZ/A, red), the sample in which Mg was added during the extrusion process (Ext. Z/A/0.5 Mg, blue), and the post-modified sample (0.5Mg/Ext. Z/A, grey).

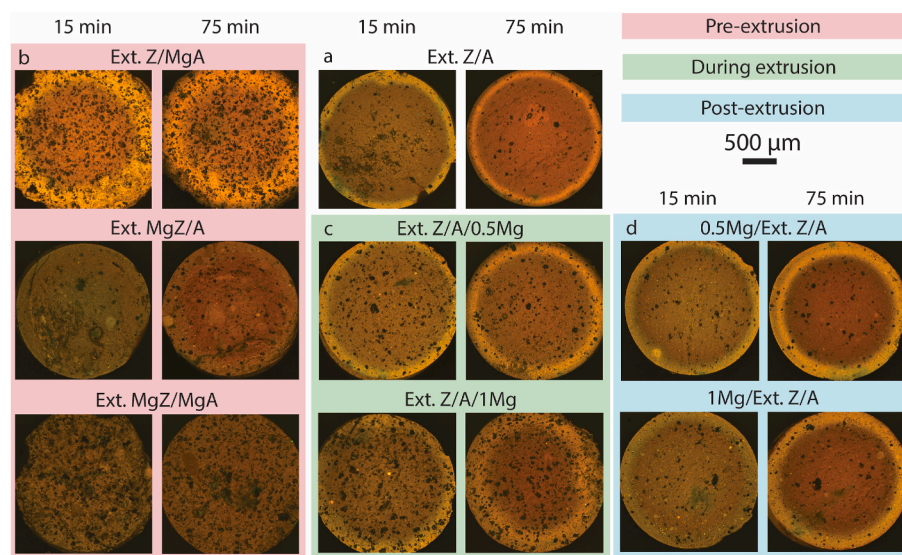


Fig. 6. Visualizing early stages of deactivation in zeolite-based shaped catalyst bodies. Confocal Fluorescence Microscopy (CFM) images of bi-sectioned spent extrudates in the Methanol-to-Hydrocarbons (MTH) reaction after 15 and 75 min Time-on-Stream (TOS) for the a) reference sample, b) pre-extrusion Mg modified samples (Ext. Z/IA, Ext. IZ/A, and Ext. IZ/IA), c) Mg added during extrusion samples (Ext. Z/A/0.5 Mg and Ext. Z/A/1 Mg), and d) post-extrusion Mg modified samples (0.5Mg/Ext. Z/A and 1Mg/Ext. Z/A).

and 1Mg/Ext. Z/A, appear to have an even darker red core region compared to the reference sample. Even though Mg impregnation on the zeolite-based catalyst extrudates decreases both weak and strong acidity, we observe a higher formation of larger hydrocarbon species in the core region of these catalyst extrudates. This could be explained by the pore narrowing and decrease in porosity, as explained previously in Fig. 1c and d.

Interestingly, pre-extrusion modification of the samples with Mg drastically changed the nature and molecular distribution of coke deposits throughout the catalyst extrudate, as demonstrated in Fig. 6b. Regarding the samples in which Mg was added only in the binder material, it still shows two areas, namely near-edge and core of the catalyst extrudates. However, the Ext. Z/MgA sample is characterized by a thicker yellow near-edge region and a red core region. The thickness of the yellow near-edge region could be explained by the smaller pore size after Mg modification, as shown in Fig. 1. The darker and/or more red hue of the two regions of interest could be attributed initially to the pore narrowing as entrapment of small molecules would be more profound. Furthermore, NH_3 -TPD analysis showed an increased acidity (for both the weak and strong acid sites) upon impregnating Mg in the alumina binder, which could increase secondary reactions of aromatic moieties and, thus, the genesis of the red fluorescence. Regarding Mg addition before extrusion in the zeolite (Ext. MgZ/A and Ext. MgZ/MgA), CFM images on the 15 min spent samples show a uniform coke formation of “less conjugated” hydrocarbon species. After 75 min TOS, conjugation into larger species is noticed, as shown from the red fluorescence emitted. The coke formation in these modified samples is vastly different from the reference sample, where two distinct areas of small and large aromatic species are formed. This is attributed to the different acidic properties of the samples. According to the literature, the formation of LAS induced by Ca or Mg modification prevents cyclic hydrocarbon pool intermediate species from participating in reactions involving aromatic moieties [30]. This could justify the existence of mainly “less conjugated” species, as the Ext. IZ/A and Ext. IZ/IA samples mainly contain weak and intermediates acid sites.

About the post-extrusion modification, as shown in Fig. 6d, a similar deactivation pattern was observed compared to the reference sample and the samples in which Mg was added during extrusion. It seems also that in this case the near-edge region of the catalyst extrudates is enlarged for both 15 and 75 min TOS. Both samples show a more red color in the core region of the catalyst extrudates, implying the dominant presence of “large conjugated” hydrocarbon species. The latter is in line with the results from the TGA measurements, which are shown in

Fig. 5c. This observation can be explained by the pore narrowing which would explain the entrapment of aromatic compounds and their further oligomerization to larger polyaromatic hydrocarbon.

Whiting et al. proved the existence of a molecular transport boundary has been proven [44]. They showed that tailoring the level of accessibility and porosity is strictly related to molecular transport. Even though the effect of the pore architecture on the molecular transport and the deactivation was established, there was no correlation on the effect of acidity. Here, our findings underlying the importance of the type of acid sites and the location of Mg in zeolite-alumina catalyst extrudates in their performance during the MTH reaction. Acidity and pore architecture are both important contributing factors in catalyst deactivation. However, acidity appears to be the most determining factor as weak and intermediate acid sites, as formed by the addition of Mg, inhibit the formation of larger polyaromatic moieties.

As shown in Fig. 7a–b, the ethylene and propylene selectivities were correlated to the changes in acidity upon Mg modification (pre-, during, and post-extrusion). The NH_3 -TPD analysis were used to calculate the amount of weak, intermediate and strong acid sites, as previously explained. Then, the concentration of each type of acid sites were calculated based on the amount of acid sites divided by the SSA of the catalyst shaped bodies, to normalize for the changes in textural properties upon Mg modification. The above mentioned approach clearly shows a linear correlation between concentration of the strong acid sites (SAS) and ethylene selectivity as well as the concentration of the weak and intermediate acid sites (WAS) and propylene selectivity. Regarding ethylene selectivity, we show that at high concentration of strong acid sites, a slight increase in the ethylene selectivity can be observed. The latter observation can be explained by the presence of strong acid sites in close proximity and to the consecutive reactions which could enhance the aromatic cycle. Simultaneously, high concentration of weak acid sites resulted in high propylene selectivity. Incorporation of Mg induced lower strong acid sites while increased the concentration of weak and intermediate acid sites, as shown in Fig. 3. The latter could lead to inhibit aromatization and coke formation, promoting the alkene cycle, and thus, propylene selectivity. Similar approach has been followed from Yarulina et al. to describe the structure-performance descriptors and to underline the role of LAS for the MTO reaction [30]. The latter research study confirms our findings.

To further understand the effect of Mg in the deactivation of zeolite-based shaped catalyst bodies, the concentration of strong acid sites was correlated to the deactivation rate calculated for each sample by the conversion over TOS. As illustrated in Fig. 7c, it is clear that there is a

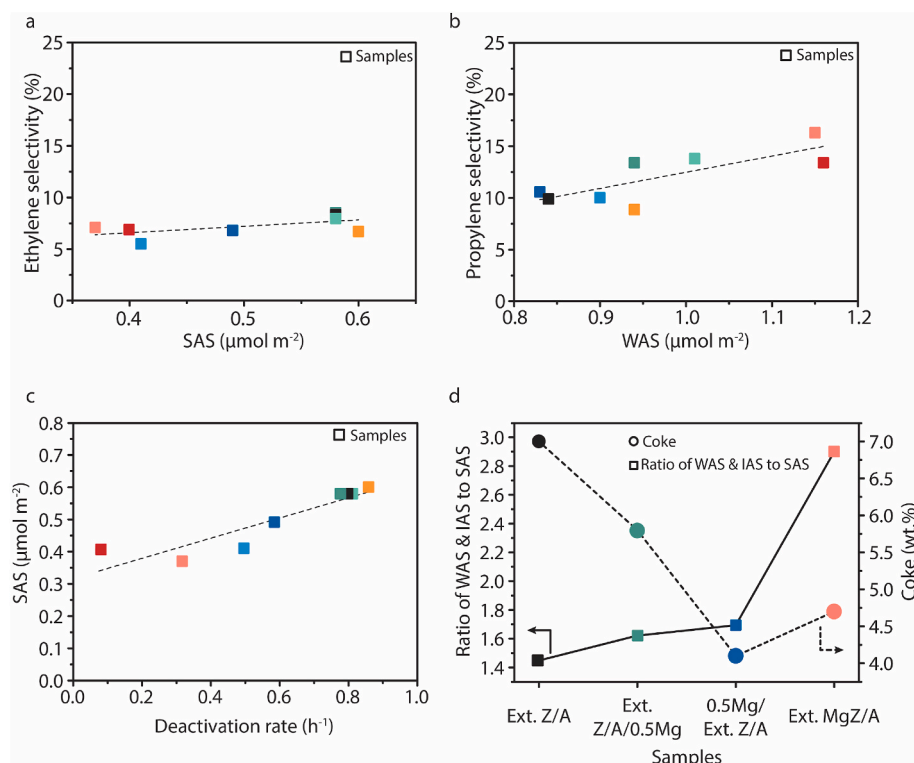


Fig. 7. Linking physicochemical properties and catalytic performance in the Methanol-to-Hydrocarbons (MTH) reaction of zeolite-based shaped catalyst bodies before and after Mg modification. Descriptors of zeolite-based shaped catalyst bodies in the MTH reaction. a) Ethylene selectivity versus strong acid sites (SAS) b) Propylene selectivity versus the weak acid sites (WAS) c) strong acid sites (SAS) versus the deactivation rate d) Ratio of the sum of weak and intermediate acid sites (IAS) and coke content after 35 h Time-on-Stream (TOS) for all samples under study. Ext. Z/A (black), Ext. MgZ/A (pink), Ext. Z/MgA (orange), Ext. MgZ/MgA (red), Ext. Z/A/0.5 Mg (green), Ext. Z/A/1 Mg (light green), 0.5Mg/Ext. Z/A (blue), and 1Mg/Ext. Z/A (light blue). The selectivities of ethylene and propylene plotted are after 1 h TOS.

linear correlation between the strong acidity and the deactivation rate. This phenomenon can be attributed to the higher formation rate of methylated aromatic species, and thus, faster coke formation due to the high amount of strong acid sites. Last but not least, the relationship between the coke content and the ratio of the sum of the concentration of weak and intermediate acid sites is shown in Fig. 7d. The reference sample, Ext. Z/A (black), with a relative low ratio of weak and intermediate to strong acid sites exhibits a high coke formation. Moving to the sample in which Mg was added during extrusion, it is obvious that coke content is reduced. Furthermore, the status is completely reversed when maximum Mg-zeolite intimacy succeeded by addition of Mg before extrusion (Ext. MgZ/A, pink). In the case of Ext. MgZ/A (pink) we see a high ratio of weak and intermediate to strong acid sites resulted relatively low coke content. We conclude that the ratio of acid sites is crucial for the coke formation and catalyst deactivation.

4. Conclusions

In this study, we have investigated the influence of the location of magnesium in zeolite-based shaped catalyst bodies on their physicochemical properties and catalytic performance in the Methanol-to-Hydrocarbons (MTH) reaction. Magnesium has been introduced in different steps of the extrusion process, namely before, during, and after the extrusion process. Physicochemical characterization of the different samples prepared proved that the pre-extrusion modification of the samples resulted in a decrease in strong acid sites, while new weak and intermediate acid sites were formed due to strong magnesium-zeolite interaction. At the same time, magnesium added prior to the extrusion process showed a significant increase in the propylene yields and the lifetime of the catalyst material prepared. A clear correlation between magnesium location, molecular transport, and catalyst deactivation during the MTH reaction of zeolite-based catalyst extrudates was made. We anticipate that this approach may contribute to designing a better catalyst material for the MTH process as well as applying this knowledge to other zeolite-based catalytic systems and acid-catalyzed chemical reactions.

CRedit authorship contribution statement

Nikolaos Nikolopoulos: Writing – review & editing, Writing – original draft, Methodology, Investigation, Formal analysis, Data curation, Conceptualization. **Luke A. Parker:** Writing – review & editing, Writing – original draft, Methodology, Investigation, Formal analysis, Data curation, Conceptualization. **Maurits W. Vuijk:** Formal analysis, Data curation. **Bert M. Weckhuysen:** Writing – review & editing, Writing – original draft, Supervision, Resources, Project administration, Funding acquisition, Conceptualization.

Declaration of competing interest

The authors declare that they have no known competing financial interests or personal relationships that could have appeared to influence the work reported in this paper.

Data availability

Data will be made available on request.

Acknowledgements

This research has received funding from the European Union's EU Framework Program for Research and Innovation Horizon 2020 under Grant Agreement No. 721385 (MSCA-ETN SOCRATES - <https://etn-socrates.eu/>) and from the US Army Research Office (ARO, with reference number W911NF-18-1-0284). Joren Dorresteyn (Utrecht University, UU), Sebastian Haben (UU), and Silvia Zanoni (UU) are acknowledged for performing the N_2 physisorption measurements. We would like to thank Dennie Wezendonk (UU) for the TGA measurements. The authors would like to thank Christia R. Jabbour (UU) for her contribution and help during the revision process.

Appendix A. Supplementary data

Supplementary data to this article can be found online at <https://doi.org/10.1016/j.micromeso.2023.112553>.

References

- [1] M. Monai, M. Gambino, S. Wannakao, B.M. Weckhuysen, Propane to olefins tandem catalysis: a selective route towards light olefins production, *Chem. Soc. Rev.* 50 (2021) 11503–11529, <https://doi.org/10.1039/d1cs00357g>.
- [2] P. Galli, G. Vecellio, Polyolefins: the most promising large-volume materials for the 21st century, *J. Polym. Sci. Part A Polym. Chem.* 42 (2004) 396–415, <https://doi.org/10.1002/pola.10804>.
- [3] M. Stöcker, Methanol-to-hydrocarbons: catalytic materials and their behavior, *Microporous Mesoporous Mater.* 29 (1999) 3–48, [https://doi.org/10.1016/S1387-1811\(98\)00319-9](https://doi.org/10.1016/S1387-1811(98)00319-9).
- [4] J.F. Haw, W. Song, D.M. Marcus, J.B. Nicholas, The mechanism of methanol to hydrocarbon catalysis, *Acc. Chem. Res.* 36 (2003) 317–326, <https://doi.org/10.1021/ar020006o>.
- [5] P. Tian, Y. Wei, M. Ye, Z. Liu, Methanol to olefins (MTO): from fundamentals to commercialization, *ACS Catal.* 5 (2015) 1922–1938, <https://doi.org/10.1021/acscatal.5b00007>.
- [6] I. Yarulina, A.D. Chowdhury, F. Meirer, B.M. Weckhuysen, J. Gascon, Recent trends and fundamental insights in the methanol-to-hydrocarbons process, *Nat. Catal.* 1 (2018) 398–411, <https://doi.org/10.1038/s41929-018-0078-5>.
- [7] L.R. Aramburo, L. Karwacki, P. Cubillas, S. Asahina, D.A.M. De Winter, M.R. Drury, L.L.C. Buurmans, E. Stavitski, D. Mores, M. Daturi, P. Bazin, P. Dumas, F. Thibault-Starzyk, J.A. Post, M.W. Anderson, O. Terasaki, B.M. Weckhuysen, The porosity, acidity, and reactivity of dealuminated zeolite ZSM-5 at the single particle level: the influence of the zeolite architecture, *Chem. Eur. J.* 17 (2011) 13773–13781, <https://doi.org/10.1002/chem.201101361>.
- [8] U. Olsbye, S. Svelle, M. Bjrgen, P. Beato, T.V.W. Janssens, F. Joensen, S. Bordiga, K. P. Lillerud, Conversion of methanol to hydrocarbons: how zeolite cavity and pore size controls product selectivity, *Angew. Chem. Int. Ed.* 51 (2012) 5810–5831, <https://doi.org/10.1002/anie.201103657>.
- [9] Z. Li, J. Martínez-Triguero, J. Yu, A. Corma, Conversion of methanol to olefins: stabilization of nanosized SAPO-34 by hydrothermal treatment, *J. Catal.* 329 (2015) 379–388, <https://doi.org/10.1016/j.jcat.2015.05.025>.
- [10] D. Mores, E. Stavitski, M.H.F. Kox, J. Kornatowski, U. Olsbye, B.M. Weckhuysen, Space- and time-resolved in-situ spectroscopy on the coke formation in molecular sieves: methanol-to-olefin conversion over H-ZSM-5 and H-SAPO-34, *Chem. Eur. J.* 14 (2008) 11320–11327, <https://doi.org/10.1002/chem.200801293>.
- [11] J. Goetze, F. Meirer, I. Yarulina, J. Gascon, F. Kapteijn, J. Ruiz-Martínez, B. M. Weckhuysen, Insights into the activity and deactivation of the methanol-to-olefins process over different small-pore zeolites as studied with operando UV-vis spectroscopy, *ACS Catal.* 7 (2017) 4033–4046, <https://doi.org/10.1021/acscatal.6b03677>.
- [12] Z. Xu, H. Ma, H. Zhang, W. Qian, W. Ying, Effect of Si/Al ratio on SSZ-13 crystallization and its methanol-to-olefins catalytic properties, *IJCME* 12 (2018) 531–535, <https://doi.org/10.5281/zenodo.1474851>.
- [13] C.D. Chang, C.T.W. Chu, R.F. Socha, Methanol conversion to olefins over ZSM-5 I. Effect of temperature and zeolite SiO₂/Al₂O₃, *J. Catal.* 86 (1984) 289–296, [https://doi.org/10.1016/0021-9517\(84\)90374-9](https://doi.org/10.1016/0021-9517(84)90374-9).
- [14] M.H.M. Ahmed, O. Muraza, M. Yoshioka, T. Yokoi, Effect of multi-step desilication and dealumination treatments on the performance of hierarchical EU-1 zeolite for converting methanol to olefins, *Microporous Mesoporous Mater.* 241 (2017) 79–88, <https://doi.org/10.1016/j.micromeso.2016.12.008>.
- [15] L.H. Ong, M. Dömök, R. Olindo, A.C. Van Veen, J.A. Lercher, Dealumination of HZSM-5 via steam-treatment, *Microporous Mesoporous Mater.* 164 (2012) 9–20, <https://doi.org/10.1016/j.micromeso.2012.07.033>.
- [16] M. Rostamizadeh, F. Yaripour, Dealumination of high silica H-ZSM-5 as long-lived nanocatalyst for methanol to olefin conversion, *J. Taiwan Inst. Chem. Eng.* 71 (2017) 454–463, <https://doi.org/10.1016/j.jtice.2016.12.003>.
- [17] M. Magomedova, E. Galanova, I. Davidov, M. Afokin, A. Maximov, Dimethyl ether to olefins over modified ZSM-5 based catalysts stabilized by hydrothermal treatment, *Catalysts* 9 (2019) 485, <https://doi.org/10.3390/catal9050485>.
- [18] M. Dusselier, M.A. Deimund, J.E. Schmidt, M.E. Davis, Methanol-to-Olefins catalysis with hydrothermally treated zeolite SSZ-39, *ACS Catal.* 5 (2015) 6078–6085, <https://doi.org/10.1021/acscatal.5b01577>.
- [19] M. Dyballa, U. Obenaus, M. Rosenberger, A. Fischer, H. Jakob, E. Klemm, M. Hunger, Post-synthetic improvement of H-ZSM-22 zeolites for the methanol-to-olefin conversion, *Microporous Mesoporous Mater.* 233 (2016) 26–30, <https://doi.org/10.1016/j.micromeso.2016.06.044>.
- [20] F.L. Bleken, K. Barbera, F. Bonino, U. Olsbye, K.P. Lillerud, S. Bordiga, P. Beato, T. V.W. Janssens, S. Svelle, Catalyst deactivation by coke formation in microporous and desilicated zeolite H-ZSM-5 during the conversion of methanol to hydrocarbons, *J. Catal.* 307 (2013) 62–73, <https://doi.org/10.1016/j.jcat.2013.07.004>.
- [21] M. Rostamizadeh, F. Yaripour, H. Hazrati, Selective production of light olefins from methanol over desilicated highly siliceous ZSM-5 nanocatalysts, *Polyolefins J* 5 (2018) 59–70, <https://doi.org/10.22063/poj.2017.1501>.
- [22] T. Fjermestad, S. Svelle, O. Swang, Mechanistic comparison of the dealumination in SSZ-13 and the desilication in SAPO-34, *J. Phys. Chem. C* 117 (2013) 13442–13451, <https://doi.org/10.1021/jp4028468>.
- [23] W. Jin, B. Wang, P. Tuo, C. Li, L. Li, H. Zhao, X. Gao, B. Shen, Selective desilication, mesopores formation, and MTO reaction enhancement via citric acid treatment of zeolite SAPO-34, *Ind. Eng. Chem. Res.* 57 (2018) 4231–4236, <https://doi.org/10.1021/acs.iecr.8b00632>.
- [24] J. Goetze, B.M. Weckhuysen, Spatiotemporal coke formation over zeolite ZSM-5 during the methanol-to-olefins process as studied with operando UV-vis spectroscopy: a comparison between H-ZSM-5 and Mg-ZSM-5, *Catal. Sci. Technol.* 8 (2018) 1632–1644, <https://doi.org/10.1039/c7cy02459b>.
- [25] I.A. Bakare, O. Muraza, M. Yoshioka, Z.H. Yamani, T. Yokoi, Conversion of methanol to olefins over Al-rich ZSM-5 modified with alkaline earth metal oxides, *Catal. Sci. Technol.* 6 (2016) 7852–7859, <https://doi.org/10.1039/c6cy00867d>.
- [26] X. Li, F. Rezaei, A.A. Rownaghi, Methanol-to-olefin conversion on 3D-printed ZSM-5 monolith catalysts: effects of metal doping, mesoporosity and acid strength, *Microporous Mesoporous Mater.* 276 (2019) 1–12, <https://doi.org/10.1016/j.micromeso.2018.09.016>.
- [27] S. Zhang, B. Zhang, Z. Gao, Y. Han, Methanol to olefin over Ca-modified HZSM-5 zeolites, *Ind. Eng. Chem. Res.* 49 (2010) 2103–2106, <https://doi.org/10.1021/ie901446m>.
- [28] H. Khezri, A. Izadbakhsh, A.A. Izadpanah, Promotion of the performance of La, Ce and Ca impregnated HZSM-5 nanoparticles in the MTO reaction, *Fuel Process. Technol.* 199 (2020), 106253, <https://doi.org/10.1016/j.fuproc.2019.106253>.
- [29] J. Valecillos, E. Epelde, J. Albo, A.T. Aguayo, J. Bilbao, P. Castaño, Slowing down the deactivation of H-ZSM-5 zeolite catalyst in the methanol-to-olefin (MTO) reaction by P or Zn modifications, *Catal. Today* 348 (2020) 243–256, <https://doi.org/10.1016/j.cattod.2019.07.059>.
- [30] I. Yarulina, K. De Wispelaere, S. Bailleul, J. Goetze, M. Radersma, E. Abou-Hamad, I. Vollmer, M. Goesten, B. Mezari, E.J.M. Hensen, J.S. Martínez-Espín, M. Morten, S. Mitchell, J. Perez-Ramirez, U. Olsbye, B.M. Weckhuysen, V. Van Speybroeck, F. Kapteijn, J. Gascon, Structure–performance descriptors and the role of Lewis acidity in the methanol-to-propylene process, *Nat. Chem.* 10 (2018) 804–812, <https://doi.org/10.1038/s41557-018-0081-0>.
- [31] M.S. Beheshti, M. Behzad, J. Ahmadpour, H. Arabi, Modification of H-[B]-ZSM-5 zeolite for methanol to propylene (MTP) conversion: Investigation of extrusion and steaming treatments on physicochemical characteristics and catalytic performance, *Microporous Mesoporous Mater.* 291 (2020), 109699, <https://doi.org/10.1016/j.micromeso.2019.109699>.
- [32] X. Jiang, X. Su, X. Bai, Y. Li, L. Yang, K. Zhang, Y. Zhang, Y. Liu, W. Wu, Conversion of methanol to light olefins over nanosized [Fe,Al]ZSM-5 zeolites: influence of Fe incorporated into the framework on the acidity and catalytic performance, *Microporous Mesoporous Mater.* 263 (2018) 243–250, <https://doi.org/10.1016/j.micromeso.2017.12.029>.
- [33] A.Z. Vazaneh, J. Towfighi, S. Sahebdehfar, Carbon nanotube templated synthesis of metal containing hierarchical SAPO-34 catalysts: impact of the preparation method and metal activities in the MTO reaction, *Microporous Mesoporous Mater.* 236 (2016) 1–12, <https://doi.org/10.1016/j.micromeso.2016.08.027>.
- [34] T.S. Zhao, T. Takemoto, N. Tsubaki, Direct synthesis of propylene and light olefins from dimethyl ether catalyzed by modified H-ZSM-5, *Catal. Commun.* 7 (2006) 647–650, <https://doi.org/10.1016/j.catcom.2005.11.009>.
- [35] Y. Song, L. lan Zhang, G. dong Li, Y. shan Shang, X. meng Zhao, T. Ma, L. ming Zhang, Y. liang Zhai, Y. jun Gong, J. Xu, F. Deng, ZSM-5 extrudates modified with phosphorus as a super effective MTP catalyst: impact of the acidity on binder, *Fuel Process. Technol.* 168 (2017) 105–115, <https://doi.org/10.1016/j.fuproc.2017.08.020>.
- [36] E.N. Biryukova, T.I. Goryainova, R.V. Kulumbegov, N.V. Kolesnichenko, S. N. Khadzhiev, Conversion of dimethyl ether into lower olefins on a La-Zr-HZSM-5/Al₂O₃ zeolite catalyst, *Petrol. Chem.* 51 (2011) 49–54, <https://doi.org/10.1134/S0965544111010026>.
- [37] F. Yaripour, Z. Shariatinia, S. Sahebdehfar, A. Irandoukht, Effect of boron incorporation on the structure, products selectivities and lifetime of H-ZSM-5 nanocatalyst designed for application in methanol-to-olefins (MTO) reaction, *Microporous Mesoporous Mater.* 203 (2015) 41–53, <https://doi.org/10.1016/j.micromeso.2014.10.024>.
- [38] C. Chen, Q. Zhang, Z. Meng, C. Li, H. Shan, Effect of magnesium modification over H-ZSM-5 in methanol to propylene reaction, *Appl. Petrochem. Res.* 5 (2015) 277–284, <https://doi.org/10.1007/s13203-015-0129-7>.
- [39] N.L. Michels, S. Mitchell, J. Pérez-Ramírez, Effects of binders on the performance of shaped hierarchical MFI zeolites in methanol-to-hydrocarbons, *ACS Catal.* 4 (2014) 2409–2417, <https://doi.org/10.1021/cs500353b>.
- [40] J. Oenema, J. Harmel, R.P. Vélaz, M.J. Meijerink, W. Eijssvogel, A. Poursaeidesfahani, T.J.H. Vlugt, J. Zečević, K.P. De Jong, Influence of nanoscale intimacy and zeolite micropore size on the performance of bifunctional catalysts for n-heptane hydroisomerization, *ACS Catal.* 10 (2020) 14245–14257, <https://doi.org/10.1021/acscatal.0c03138>.
- [41] J. Zečević, G. Vanbutsel, K.P. De Jong, J.A. Martens, Nanoscale intimacy in bifunctional catalysts for selective conversion of hydrocarbons, *Nature* 528 (2015) 245–254, <https://doi.org/10.1038/nature16173>.
- [42] K. Cheng, L.I. van der Wal, H. Yoshida, J. Oenema, J. Harmel, Z. Zhang, G. Sunley, J. Zečević, K.P. de Jong, Impact of the spatial organization of bifunctional metal-zeolite catalysts on the hydroisomerization of light Alkanes, *Angew. Chem. Int. Ed.* 59 (2020) 3592–3600, <https://doi.org/10.1002/anie.201915080>.
- [43] Y. Wang, G. Wang, L.I. van der Wal, K. Cheng, Q. Zhang, K.P. de Jong, Y. Wang, Visualizing element migration over bifunctional metal-zeolite catalysts and its impact on catalysis, *Angew. Chem. Int. Ed.* 60 (2021) 17735–17743, <https://doi.org/10.1002/anie.202107264>.
- [44] G.T. Whiting, N. Nikolopoulos, I. Nikolopoulos, A.D. Chowdhury, B. M. Weckhuysen, Visualizing pore architecture and molecular transport boundaries

- in catalyst bodies with fluorescent nanopores, *Nat. Chem.* 11 (2019) 23–31, <https://doi.org/10.1038/s41557-018-0163-z>.
- [45] L. Chen, Y. Xu, B. Wang, J. Yun, F. Dehghani, Y. Xie, X. Liang, Mg-modified CoMo/Al₂O₃ with enhanced catalytic activity for the hydrosulfurization of 4, 6-dimethyldibenzothiophene, *Catal. Commun.* 155 (2021), 106316, <https://doi.org/10.1016/j.catcom.2021.106316>.
- [46] G. Zhao, J. Teng, Z. Xie, W. Jin, W. Yang, Q. Chen, Y. Tang, Effect of phosphorus on HZSM-5 catalyst for C₄-olefin cracking reactions to produce propylene, *J. Catal.* 248 (2007) 29–37, <https://doi.org/10.1016/j.jcat.2007.02.027>.
- [47] E.A. Uslamin, B. Luna-Murillo, N. Kosinov, P.C.A. Bruijninx, E.A. Pidko, B. M. Weckhuysen, E.J.M. Hensen, Gallium-promoted HZSM-5 zeolites as efficient catalysts for the aromatization of biomass-derived furans, *Chem. Eng. Sci.* 198 (2019) 305–316, <https://doi.org/10.1016/j.ces.2018.09.023>.
- [48] N. Nikolopoulos, R.G. Geitenbeek, G.T. Whiting, B.M. Weckhuysen, Unravelling the effect of impurities on the methanol-to-olefins process in waste-derived zeolites ZSM-5, *J. Catal.* 396 (2021) 136–147, <https://doi.org/10.1016/j.jcat.2021.02.015>.
- [49] Y. Wang, Y. Chang, M. Liu, A. Zhang, X. Guo, A facile strategy to prepare shaped ZSM-5 catalysts with enhanced para-xylene selectivity and stability for toluene methylation: the effect of in situ modification by attapulgite, *Molecules* 24 (2019) 3462, <https://doi.org/10.3390/molecules24193462>.
- [50] G.T. Whiting, A.D. Chowdhury, R. Oord, P. Paalanen, B.M. Weckhuysen, The curious case of zeolite-clay/binder interactions and their consequences for catalyst preparation, *Faraday Discuss* 188 (2016) 369–386, <https://doi.org/10.1039/c5fd00200a>.
- [51] X. Di Chen, X.G. Li, H. Li, J.J. Han, W. De Xiao, Interaction between binder and high silica HZSM-5 zeolite for methanol to olefins reactions, *Chem. Eng. Sci.* 192 (2018) 1081–1090, <https://doi.org/10.1016/j.ces.2018.08.047>.
- [52] G.T. Whiting, S.H. Chung, D. Stosic, A.D. Chowdhury, L.I. Van Der Wal, D. Fu, J. Zecevic, A. Travert, K. Houben, M. Baldus, B.M. Weckhuysen, Multiscale mechanistic insights of shaped catalyst body formulations and their impact on catalytic properties, *ACS Catal.* 9 (2019) 4792–4803, <https://doi.org/10.1021/acscatal.9b00151>.
- [53] K. Yang, D. Zhang, M. Zou, L. Yu, S. Huang, The known and overlooked sides of zeolite-extrudate catalysts, *ChemCatChem* 13 (2021) 1414–1423, <https://doi.org/10.1002/cctc.202001601>.
- [54] B. Luna-Murillo, M. Pala, A.L. Paioni, M. Baldus, F. Ronsse, W. Prins, P.C. A. Bruijninx, B.M. Weckhuysen, Catalytic fast pyrolysis of biomass: catalyst characterization reveals the feed-dependent deactivation of a technical ZSM-5-based catalyst, *ACS Sustain. Chem. Eng.* 9 (2021) 291–304, <https://doi.org/10.1021/acssuschemeng.0c07153>.